Journal of Power Sources 195 (2010) 3668–3675

Contents lists available at ScienceDirect

Journal of Power Sources

journal homepage: www.elsevier.com/locate/jpowsour

Ternary polymer electrolytes containing pyrrolidinium-based polymeric ionic liquids for lithium batteries

G.B. Appetecchi[a,*], G.-T. Kim[a], M. Montanino[a], M. Carewska[a], R. Marcilla[b,**], D. Mecerreyes[b], I. De Meatza[b]

[a] ENEA, IDROCOMB, Casaccia Research Center, Via Anguillarese 301, 00123 Rome, Italy
[b] CIDETEC, Centro de Tecnologías Electroquímicas, Parque Tecnológico de San Sebastián, Paseo Miramón, 196 20009 Donostia-San Sebastián, Spain

ARTICLE INFO

Article history:
Received 25 September 2009
Received in revised form
24 November 2009
Accepted 27 November 2009
Available online 30 December 2009

Keywords:
Pyrrolidinium ionic liquids
Poly(diallyldimethylammonium) bis(trifluoromethanesulfonyl)imide
N-Butyl-*N*-methylpyrrolidinium bis(trifluoromethanesulfonyl)imide
Polymer electrolytes
Lithium polymer batteries

ABSTRACT

The electrochemical properties of solvent-free, ternary polymer electrolytes based on a novel poly(diallyldimethylammonium) bis(trifluoromethanesulfonyl)imide polymeric ionic liquid (PIL) as polymer host and incorporating $PYR_{14}TFSI$ ionic liquid and LiTFSI salt are reported. The PIL–LiTFSI–$PYR_{14}TFSI$ electrolyte membranes were found to be chemically stable even after prolonged storage times in contact with lithium anode and thermally stable up to 300 °C. Particularly, the PIL-based electrolytes exhibited acceptable room temperature conductivity with wide electrochemical stability window, time-stable interfacial resistance values and good lithium stripping/plating performance. Preliminary battery tests have shown that Li/$LiFePO_4$ solid-state cells are capable to deliver above 140 mAh g^{-1} at 40 °C with very good capacity retention up to medium rates.

1. Introduction

Lithium metal polymer batteries (LMPBs) are considered excellent candidates for the next generation power sources due to their high energy density and flexible characteristics [1]. Nevertheless, the performance of LMPBs is still limited by the relatively low ionic conductivity of solvent-free, polymer electrolytes (SPEs) at room temperature [2].

In this scenario, the addition of non-flammable, non-volatile, room temperature ionic liquid (RTILs) into polymer electrolytes represents a very promising approach. Since their high ionic conductivity and electrochemical stability, RTILs have been also largely investigated as electrolyte (or electrolyte components) for several electrochemical applications [3–20] including rechargeable lithium batteries. Particularly, RTILs formed by *N*-alkyl-*N*-methylpyrrolidinium cations $(PYR_{1A})^+$ (the subscripts indicate the number of carbons in the alkyl side chains) and bis(trifluoromethanesulfonyl)imide $(TFSI)^-$ anions have been proposed as electrolyte components for LMBPs [21–23]. Furthermore, pyrrolidinium cations show a much wider cathodic decomposition potential compared to non-cyclic and unsaturated cyclic quaternary ammonium cations [24] that, also, have an unfavorable compatibility towards the lithium metal anode due to the presence of acidic protons and double bonds in the cation [25].

Mainly, two different approaches have been followed in the attempt to transfer the favorable properties of ionic liquids into LMPB systems. The first one is the incorporation of RTILs into polymer electrolytes. Following this approach, we have successfully demonstrated [16–20,26,27] that the addition of $PYR_{1A}TFSI$ enhances the ionic conductivity of PEO-based electrolytes above 10^{-4} S cm^{-1} at room temperature without any decrease of the electrochemical stability window of the polymer electrolyte.

The second approach consists in synthesizing functional polymeric materials through polymerization of ionic liquid monomers to be used as matrices for polymer electrolyte systems [28–32]. These materials, hereafter named polymeric ionic liquids (PILs), exhibit interesting properties as tunable solubility, good ionic conductivity and chemical compatibility towards ionic liquids. The use of PILs as matrices in ionic liquid-based polymer electrolytes presents some advantages comparing with other polymer hosts. Firstly, the chemical affinity between PILs and ILs affords a completely compatible combination resulting in stable polymer electrolytes. This allows a completely well-suited and tuneable blend, thus minimizing phase separation and leakage phenom-

* Corresponding author. Tel.: +39 06 3048 3924; fax: +39 06 3048 6357.
** Corresponding author. Tel.: +34 943309022; fax: +34 943309136.
E-mail addresses: gianni.appetecchi@enea.it (G.B. Appetecchi), rmarcilla@cidetec.es (R. Marcilla).

0378-7753/$ – see front matter © 2009 Elsevier B.V. All rights reserved.
doi:10.1016/j.jpowsour.2009.11.146

ena. Beneficial aspects in electrochromic devices, including the significant enhancement in cyclability and durability, have been reported elsewhere [28]. Secondly, the electrochemical stability and the ionic character of PILs make them excellent candidates as electrolyte hosts even at severe potentials. Finally, PIL-based electrolytes are easy to process, especially in view of industrial applications.

In a previous work [32] we have prepared and characterized several kinds of poly(dyallildimethylammonium)-based PILs with different counter-ions. Among these, the materials based on bis(trifluoromethanesulfonyl)imide ($TFSI^-$) anion showed very good performance as host for polymer electrolytes in combination with $PYR_{14}TFSI$ ionic liquid and LiTFSI salt. In the present paper, we report the results of the investigation on ternary polymer electrolytes based on poly(dyallildimethylammonium) bis(trifluoromethanesulfonyl)imide (PIL), $PYR_{14}TFSI$ and LiTFSI. Various sets of PIL–LiTFSI–$PYR_{14}TFSI$ electrolyte membranes having different weight compositions were prepared and physicochemically investigated. Finally, the PIL–LiTFSI–$PYR_{14}TFSI$ tapes were used as electrolyte separators in LMPBs at low-medium temperatures.

2. Experimental

2.1. Synthesis of $PYR_{14}TFSI$ ionic liquid

The $PYR_{14}TFSI$ ionic liquid was synthesized through a procedure developed at ENEA and described in details elsewhere [33]. The synthetic route allowed to obtain high purity (>99.5 wt.%), colorless and odorless $PYR_{14}TFSI$ with a humidity content lower than 2 ppm. The water content in the ionic liquid was measured by an automatic Karl Fisher coulometer titrator (Mettler Toledo DL32) in dry-room (R.H. <0.1%) at 20 °C. The Karl Fisher titrant was a one-component (Hydranal 34836 Coulomat AG) reagent purchased from Aldrich.

2.2. Synthesis of pyrrolidinium-based polymeric ionic liquid (PIL)

Polymeric ionic liquid (PIL) containing pyrrolidinium pendant units and TFSI as counteranion was synthesized through anion exchange reaction from the commercially available polymer poly(diallyldimethylammonium) chloride (Aldrich, average Mw 400,000–500,000, 20 wt.% in H_2O). The procedure developed at CIDETEC is described in details elsewhere [32]. The reactants poly(diallyldimethylammonium) chloride solution and LiTFSI (≥99 wt.%) were purchased from Aldrich and Fluka, respectively, and used as received. The procedure allowed to obtain high purity, white, solid poly(diallyldimethylammonium) bis(trifluoromethanesulfonyl)imide with high yields (93.5%). The chemical structure of PIL is depicted in Fig. 1, panel A.

2.3. Preparation of solid polymer electrolytes and cathode tapes

The ternary polymer electrolytes were prepared by separately dissolving PIL (host), $PYR_{14}TFSI$ (ionic liquid) and LiTFSI (salt) in acetone and, then, mixed in three different proportions (Table 1). Cathodes were obtained by intimately mixing $LiFePO_4$ (Südchemie, active material, 43 wt.%), carbon (Super-P, Timcal, 7 wt.%) and PIL–LiTFSI–$PYR_{14}TFSI$ ternary polymer electrolyte (50 wt.%), e.g., the last having the same composition of the set C separator used in full batteries (Fig. 11), in acetone and vigorously stirring overnight. The electrolyte and cathodic slurries were casted by doctor blade. The solvent was allowed to slowly evaporate at room temperature to obtain free-standing, homogeneous, transparent polymer electrolyte membranes (55–60 μm thick) and composite cathode tapes (70 μm thick). Finally, the PIL-based electrolyte membranes as well as the cathode tapes were dried under high vacuum (10^{-5} mbar) at 100 °C for three days in dry-room. Different PIL–LiTFSI–$PYR_{14}TFSI$ sample sets were prepared with a $PYR_{14}TFSI$ content ranging from 43.8 to 60.0 wt.% (Table 1) while the LiTFSI amount was fixed to 12.4 wt.%. A picture of a PIL–LiTFSI–$PYR_{14}TFSI$ electrolyte membrane sample (set C) is depicted in Fig. 1, panel B.

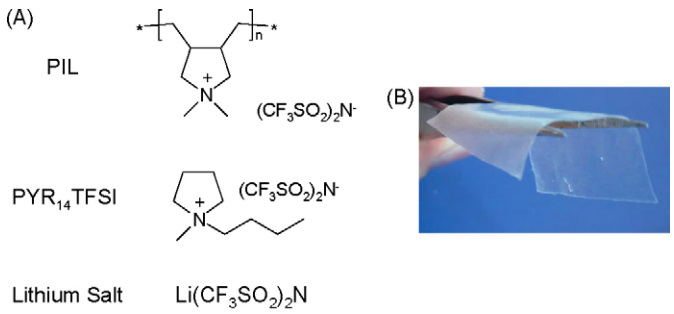

Fig. 1. Panel A: chemical structure of the components of PIL–LiTFSI–$PYR_{14}TFSI$ ternary polymer electrolytes. Panel B: picture of a PIL–LiTFSI–$PYR_{14}TFSI$ sample.

2.4. Thermal analysis

Differential scanning calorimetry (DSC) measurements were performed using a thermal analyzer system TA Instruments Q 100 DSC at a heating rate of 10 °C min^{-1} with a 50 mL min^{-1} helium flow rate. The samples (about 5 mg) were sealed in aluminum DSC pan inside the dry-room. Typically the samples were cooled at 10 °C min^{-1} from room temperature to −140 °C and, then, heated at 10 °C min^{-1} up to 100 °C.

The thermal stability was verified by a Q 600 SDT equipment, simultaneous TG-DTA (TA Instruments) with Thermal Solution Software (version 1.4). A high purity calcined aluminium oxide was used as the reference material. The samples (10–12 mg) were stored, handled and weighed in dry-room. The thermal stability was investigated by heating the samples from ambient temperature to 700 °C at a 10 °C min^{-1} heating rate. During the tests synthetic air or nitrogen was flown at a 100 ml min^{-1} flow rate.

2.5. Test cells assembly

The electrochemical measurements on the PIL–LiTFSI–$PYR_{14}TFSI$ ternary polymer electrolytes were performed on two-electrode cells fabricated in dry-room. The test cells (active area equal to 1–2 cm^2) were assembled by sandwiching a PIL electrolyte sample between two copper (conductivity

Table 1
Composition of PIL–LiTFSI–$PYR_{14}TFSI$ ternary polymer electrolytes. The $PYR_{14}TFSI$/PIL and $PYR_{14}TFSI$/LiTFSI ratios (in weight and in mole) are reported for comparison.

Sample set	Weight composition (wt.%)			$PYR_{14}TFSI$/PIL ratio		$PYR_{14}TFSI$/LiTFSI ratio	
	PIL	$PYR_{14}TFSI$	LiTFSI	wt/wt	mole/mole	wt/wt	mole/mole
Set A	43.8	43.8	12.4	1.00	0.97	3.53	2.40
Set B	37.6	50.0	12.4	1.33	1.29	4.03	2.74
Set C	27.6	60.0	12.4	2.17	2.10	4.84	3.29

[a] PIL monomer.

measurements) or lithium (Li/electrolyte interfacial stability and lithium stripping-plating measurements) foils or between (linear sweep voltammetry tests) a nickel (working electrode; 0.10 mm thick) and a lithium (counter and reference electrode; 0.05 mm thick) foils. The assembled cells as well as the full batteries were housed in vacuum-sealed, coffee-bag envelopes and successively laminated twice by hot-rolling at 100 °C.

All-solid-state Li/$LiFePO_4$ batteries (cathode limited) were fabricated (in dry-room) by laminating a lithium foil (50 μm), a PIL–LiTFSI–PYR_{14}TFSI ternary polymer electrolyte membrane and a $LiFePO_4$ cathode tape. The electrochemical active area of the laminated cells approached 1 cm^2. The active material mass loading levelled 5.5 mg cm^{-2}, corresponding to 0.93 mAh cm^{-2}.

2.6. Electrochemical tests

The ionic conductivity of the PIL–LiTFSI–PYR_{14}TFSI ternary polymer electrolytes and their interfacial stability with lithium metal anode were determined by impedance measurements taken on Cu/SPE/Cu or Li/SPE/Li cells, respectively. The AC tests were performed by means of a Frequency Response Analyzer (F.R.A., Schlumberger Solartron 1260) in the 1 Hz–100 kHz (conductivity tests) and 0.1 Hz–100 kHz (interfacial stability tests) frequency ranges, respectively.

The conductivity tests were performed on a heating stepped ramp from −40 to 100 °C. Prior to performing the temperature ramp, the Cu/SPE/Cu cells were held at −40 °C for 24 h to avoid slow kinetic effects on the polymer electrolytes. The temperature was changed in 10 °C steps every 24 h to allow for a complete thermal equilibration of the cells before each measurement. The interfacial stability measurements were taken for a storage time higher than 3 months at different temperature. Initially, the cells were stored at 20 °C for 31 days. After this period, the storage temperature was increased up to 40 °C for 23 days and, then, again reduced at 20 °C for additional 40 days. The test cells were located in a cold/heat test chamber Binder GmbH MK53 with a temperature control of ±0.1 °C. The impedance responses were analyzed using the well-known non-linear least-square (NLLSQ) fit software [34,35] on the basis of a suitable equivalent circuit model [36]. All measurements were carried out on at least three different cells for each polymer electrolyte sample in order to verify the reproducibility of the obtained results.

The cyclability of lithium metal electrodes in PIL–LiTFSI–PYR_{14}TFSI ternary polymer electrolytes was evaluated using a MACCOR S4000 battery cycler by stripping/plating tests on two-electrode, symmetric, Li/SPE/Li cells at 40 °C. The test consisted in flowing a constant current (0.05 mA cm^{-2}) through the cells, but its polarity was reversed every 1 h. The cyclability at the Li/PIL–LiTFSI–PYR_{14}TFSI interface was followed by recording the cell overvoltage during the galvanostatic tests where each electrode alternatively acts as source and sink of lithium ions moving in the polymer electrolyte.

The electrochemical stability window (ESW) of the PIL–LiTFSI–PYR_{14}TFSI electrolytes was evaluated by linear sweep voltammetries (LSVs) at 0.5 mV s^{-1}. The measurements were performed scanning the cell voltage from the open circuit value (OCV) towards more negative or positive voltages to determine the cathodic and anodic electrochemical stability limits, respectively. The LSVs were performed at least twice on each electrolyte sample to confirm the results obtained using fresh samples and clean electrodes for each test. The measurements were performed at 40 °C using a Schlumberger (Solartron) Electrochemical Interface (model 1287) controlled by a software developed at ENEA.

Preliminary cycling tests on Li/$LiFePO_4$ polymer batteries were performed at 40 °C using a MACCOR S4000 battery tester. The discharge current rates were ranged from C/20 (0.044) to 2C (1.8 mA cm^{-2}) while the charge rate was fixed to C/20. The voltage cut-offs were fixed at 4.0 V (charge step) and 2.0 V (discharge step), respectively.

3. Results and discussion

The PIL–LiTFSI–PYR_{14}TFSI ternary polymer electrolytes showed good mechanical properties even at large ionic liquid contents (set C) with high adhesion onto several materials, this allowing a good contact at the interface with electrodes. Unfortunately, it was impossible to measure directly the water content in PIL electrolytes since they do not dissolve in the analytic Karl Fisher solution (no water was detected but it could depend on the low water release kinetics). However, calculations based on the total charge involved in the 0.8 V vs. Li/Li^+ cathodic peak of Fig. 6 indicated a water content below 30 ppmw.

3.1. Chemical stability

The chemical stability of the PIL–LiTFSI–PYR_{14}TFSI electrolytes was evaluated by following the time evolution of the impedance response of Li/polymer electrolyte/Li cells stored at different temperatures. Fig. 2 magnifies the AC responses of a Li/PIL–LiTFSI–PYR_{14}TFSI (set C)/Li cell in the high frequency region. The intercept of the AC plots with the real axis corresponds to the electrolyte resistance [36]. No change of the AC plot feature and of the bulk ionic resistance was observed. This indicates that no degradation phenomenon takes place within the PIL–LiTFSI–PYR_{14}TFSI electrolytes even after prolonged storage times (92 days) and heating/cooling steps in contact with lithium metal. The results reported in Table 3 and plotted in Fig. 9 (time evolution of electrolyte resistance) supports this issue.

3.2. Thermal analysis

The thermal properties of the PIL–LiTFSI–PYR_{14}TFSI ternary polymer electrolytes have been investigated by DSC (Fig. 3) and TGA (Fig. 4) measurements. As evidenced in Fig. 3, the pure ionic liquid exhibits just a sharp endothermic peak at −5 °C due to the melting

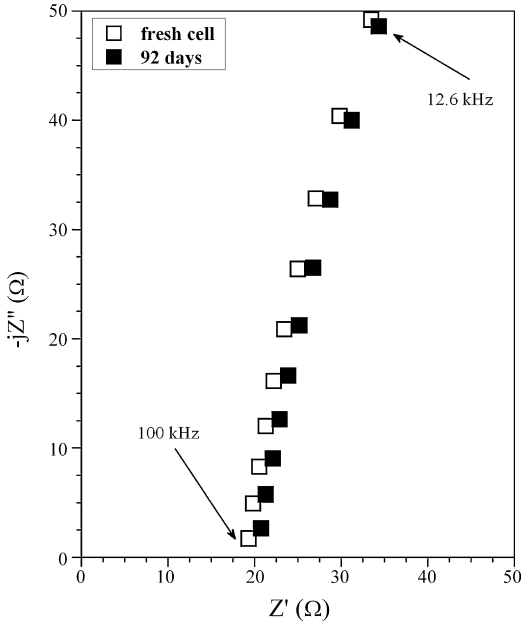

Fig. 2. High frequency range of the AC impedance response of a Li/PIL–LiTFSI–PYR_{14}TFSI/Li cell taken at different storage times. T = 20 °C.

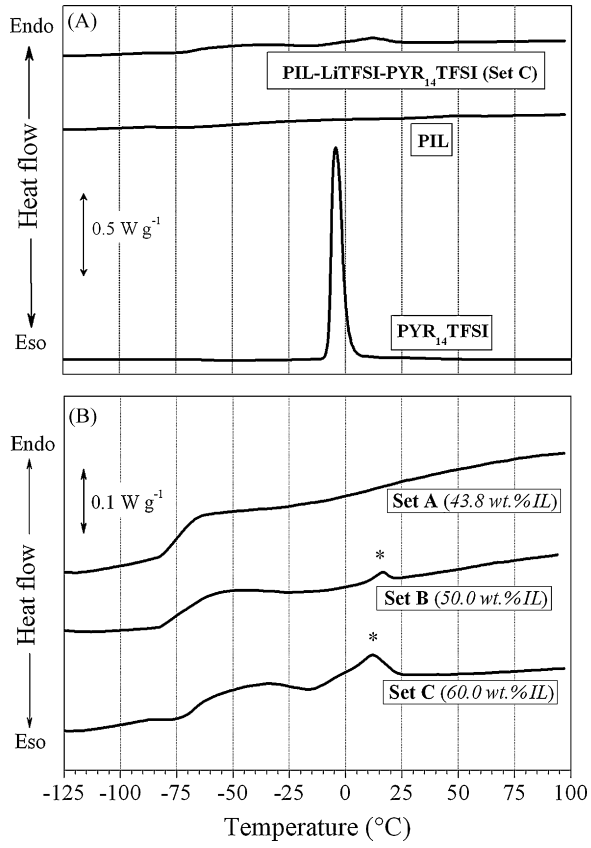

Fig. 3. Panel A: DSC trace of neat PIL polymer, neat $PYR_{14}TFSI$ ionic liquid and a PIL–LiTFSI–$PYR_{14}TFSI$ (set C) sample. Scan rate: 10 °C min^{-1}. Panel B: DSC trace of different PIL–LiTFSI–$PYR_{14}TFSI$ samples. Scan rate: 10 °C min^{-1}.

of the material [23], whereas neat PIL and the PIL–LiTFSI–$PYR_{14}TFSI$ sample exhibit a glass transition feature (T_g) around −67 °C. Panel B of Fig. 3 depicts the DSC trace of PIL–LiTFSI–$PYR_{14}TFSI$ electrolytes at different ionic liquid contents. The $PYR_{14}TFSI$ amount does not affect the glass phase transition whereas no other feature is exhibited up to an ionic liquid content equal to about 44 wt.%. At higher IL amounts, a small endothermic peak is observed at around 17 °C (set B) and 12 °C (set C). This feature was found to increase with increasing the ionic liquid content, and may be likely addressed to the melting of some excess of LiTFSI–$PYR_{14}TFSI$ phase [14], this suggesting a lithium salt/ionic liquid phase separation within PIL–LiTFSI–$PYR_{14}TFSI$ electrolytes above a $PYR_{14}TFSI$ content equal to 44 wt.%. Also, the shift of the peak from about 17 °C (set B) to 12 °C (set C) with the increasing of the ionic liquid amount suggests a change of the composition of the LiTFSI–$PYR_{14}TFSI$ phase excess. The comparison with the LiTFSI–$PYR_{14}TFSI$ binary system diagram clearly indicates that this phase excess shows a larger ionic liquid content [37]. It is worthy to note that no visible liquid leakage was observed on the surface of the PIL ternary electrolyte membranes even after prolonged storage times.

Fig. 4 illustrates the TGA trace of a PIL–LiTFSI–$PYR_{14}TFSI$ (set C) electrolyte membrane and pure PIL and $PYR_{14}TFSI$ for comparison purpose. As shown in the figure, the PIL–LiTFSI–$PYR_{14}TFSI$ sample exhibits a similar thermal behavior with respect to the pure components. Apart from an initial small weight loss (about 1 wt.% up to 70 °C) due to water removal (e.g., TGA measurements were performed in not controlled environment), the PIL-based electrolyte samples were found to be thermally stable up to 300 °C both in air and nitrogen atmosphere.

3.3. Conductivity measurements

Fig. 5 compares the conductivity vs. temperature dependence of different PIL–LiTFSI–$PYR_{14}TFSI$ electrolytes. The pure $PYR_{14}TFSI$, reported for comparison purpose, shows two linear trends with a sharp conductivity jump at −5 °C due to the melting of the material [23]. The PIL-based electrolyte samples exhibited a different conductivity vs. temperature behavior with a knee around 10 °C for sets A and B and around 0 °C for set C, likely due to the salt rich phase [2]. Above the slope change, the PIL-based electrolytes exhibit a VTF-like behavior [38], typically observed in completely amorphous ionic conductors [39–41]. Below the conductivity knee, the polymer samples exhibit a linear trend with similar slope, this indicating close activation energy values for the low temperature conduction process [41–43]. As clearly evidenced from Fig. 5, the ionic conductivity is found to progressively increase with increasing the ionic liquid content, especially at low-medium temperatures, as well as the slope change shifts from 10 to 0 °C. At 20 °C the set C polymer electrolyte shows a conductivity higher than 1.6×10^{-4} S cm^{-1} (Table 2) that approaches 5×10^{-4} S cm^{-1} and 1×10^{-3} S cm^{-1} at 40 and 60 °C, respectively. These values match the ones observed for analogous ionic liquid-based polymer electrolyte membranes [18,26]. Also interesting to point out is that the low temperature

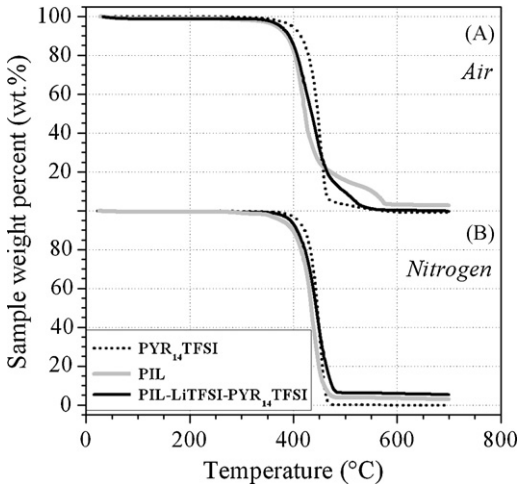

Fig. 4. TGA trace of neat PIL, neat $PYR_{14}TFSI$ and a PIL–LiTFSI–$PYR_{14}TFSI$ (set C) sample in air (panel A) and nitrogen (panel B) atmosphere. Scan rate: 10 °C min^{-1}.

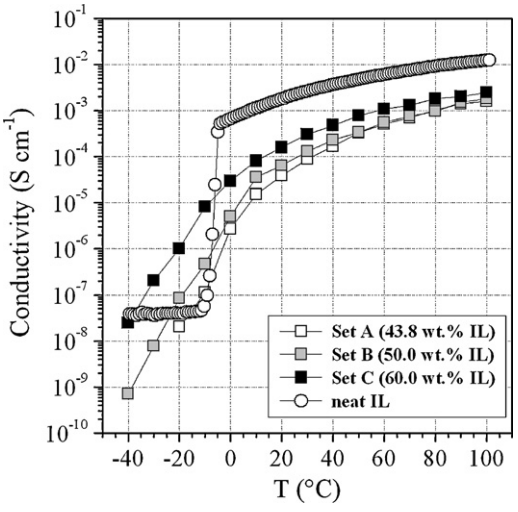

Fig. 5. Ionic conductivity vs. temperature dependence of PIL–LiTFSI–$PYR_{14}TFSI$ electrolytes at different IL content. The data referred to neat $PYR_{14}TFSI$ ionic liquid (from Ref. [23]) are reported for comparison purpose.

Table 2
Electrochemical properties of PIL–LiTFSI–$PYR_{14}TFSI$ ternary polymer electrolytes.

Sample set	Conductivity ($S\,cm^{-1}$)		Li/SPE resistance ($\Omega\,cm^2$)	
	20 °C	40 °C	20 °C	40 °C
Set A	$(3.8 \pm 0.6) \times 10^{-5}$	$(1.7 \pm 0.2) \times 10^{-4}$	2400 ± 300	380 ± 50
Set B	$(6.4 \pm 0.9) \times 10^{-5}$	$(2.3 \pm 0.3) \times 10^{-4}$	n.d.	n.d.
Set C	$(1.6 \pm 0.2) \times 10^{-4}$	$(4.8 \pm 0.7) \times 10^{-4}$	2200 ± 300	280 ± 30

(below −10 °C) conductivity of the PIL-based electrolyte systems is higher than that of the neat ionic liquid and its mixtures with LiTFSI (data not reported). We can suppose that the PIL polymer host is able to interact with the lithium salt and ionic liquid, thus preventing the formation of the 0.33LiTFSI–0.66 $PYR_{14}TFSI$ crystalline phase [44,45] and, therefore, enhancing the ionic conductivity of the ternary polymer electrolyte. This issue is in good agreement with the thermal measurements of Fig. 3.

3.4. Electrochemical stability

The electrochemical stability window of the PIL–LiTFSI–$PYR_{14}TFSI$ ternary polymer electrolytes was measured as function of the ionic liquid content (Fig. 6A) at different temperatures (Fig. 6B). The ionic liquid content does not affect the electrochemical stability of the PIL-based electrolytes that exhibited an ESW from the lithium plating to above 5.0 V vs. Li^+/Li° at 20 °C and about 4.9 V vs. Li^+/Li at 40 °C. A very low current flow (<2 $\mu A\,cm^{-2}$) was observed up to the anodic break-down voltage, thus supporting for the high purity of the PIL-based electrolytes.

On the cathodic verse, three weak ($\leq 25\,\mu A\,cm^{-2}$) peaks are observed around 1.5, 0.8 and 0.5 V vs. Li^+/Li°, respectively. These features are found to increase with the temperature (panel A) and ionic liquid content (panel B) since the corresponding increase in ionic conductivity (Fig. 5) of the electrolyte sample. For clarifying the nature of such features, consecutive cyclic voltammetries were performed within the 0.1–3.0 V range (Fig. 7) that did not lead to the complete disappearance of the cathodic profiles, thus indicating some reversible process taking place in the cell. From data reported in literature, we can assign the peaks at 1.5 and 0.5 V vs. Li^+/Li° to the more or less reversible intercalation process of Li^+ cations into native Ni_xO film on the nickel working electrode surface [46]. The peak at 0.8 V vs. Li^+/Li° is likely due to water impurities.

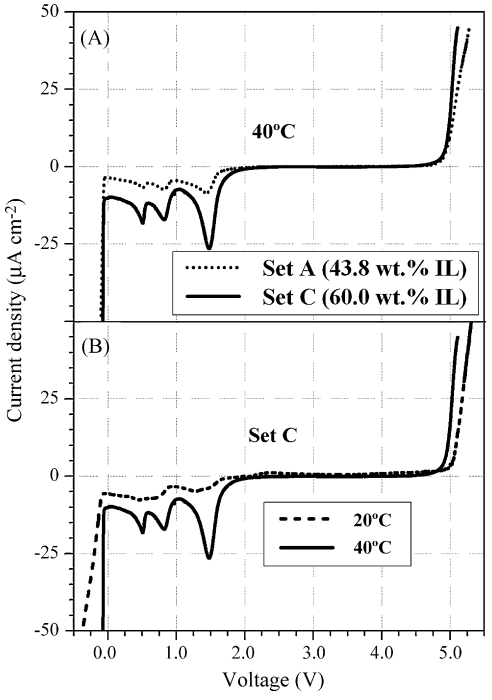

Fig. 6. Electrochemical stability window of different PIL–LiTFSI–$PYR_{14}TFSI$ electrolytes at 40 °C (panel A) and a set C PIL–LiTFSI–$PYR_{14}TFSI$ sample at different temperatures (panel B). Nickel and lithium as working and counter electrodes, respectively. Scan rate: 0.5 $mV\,s^{-1}$.

3.5. Interfacial properties

The interfacial properties of the PIL–LiTFSI–$PYR_{14}TFSI$ electrolytes with the lithium anode were evaluated by following the time evolution of the impedance response of symmetrical Li/polymer electrolyte/Li cells stored at different temperatures (Fig. 8). The PIL-based electrolytes showed a slightly depressed semicircle, associated with the lithium–polymer electrolyte interfacial processes [36]. The diameter of the semicircle is related with the overall interfacial resistance (R_i) that takes into account the charge transfer resistance at the Li/electrolyte interface (R_{ct}) as well as the additional impedance (R_P) associated with the growth of a passive layer, e.g., $R_i = R_{ct} + R_P$. The shape of the impedance responses does not substantially change with the temperature. However, a relevant reduction of the semicircles is observed on increasing the cell temperature from 20 to 40 °C. The equivalent circuit proposed to represent the electrochemical cells under study is depicted in panel C of Fig. 8.

Table 3 reports the normalized R_b, R_{ct} and R_p resistance values for a PIL–LiTFSI–$PYR_{14}TFSI$ (set C) sample in contact with a lithium anode at different storage times and temperatures. The time evolution of the normalized interface resistance (R_i) of PIL–LiTFSI–$PYR_{14}TFSI$ samples at different ionic liquid contents is also depicted in Fig. 9. The electrolyte resistance values are in good agreement with the conductivity data depicted in Fig. 5 and reported in Table 2. During the initial period of storage at 20 °C, a marked increase of R_i was observed while in the following part of the test (3 months) the interfacial resistance was found to be constant, leveling at 2000 $\Omega\,cm^2$ after 20 days storage. This behavior,

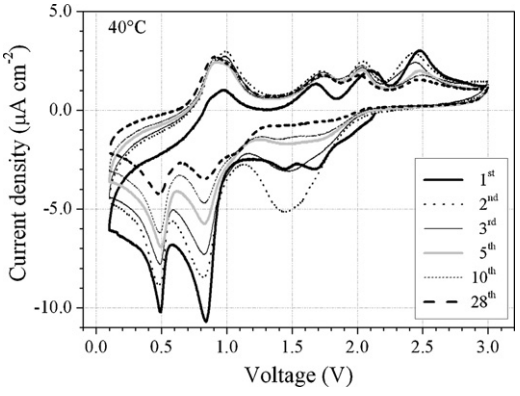

Fig. 7. Cyclic voltammetries on a PIL–LiTFSI–$PYR_{14}TFSI$ (set C) electrolyte at 40 °C. Nickel and lithium as working and counter electrodes, respectively. Scan rate: 0.5 $mV\,s^{-1}$.

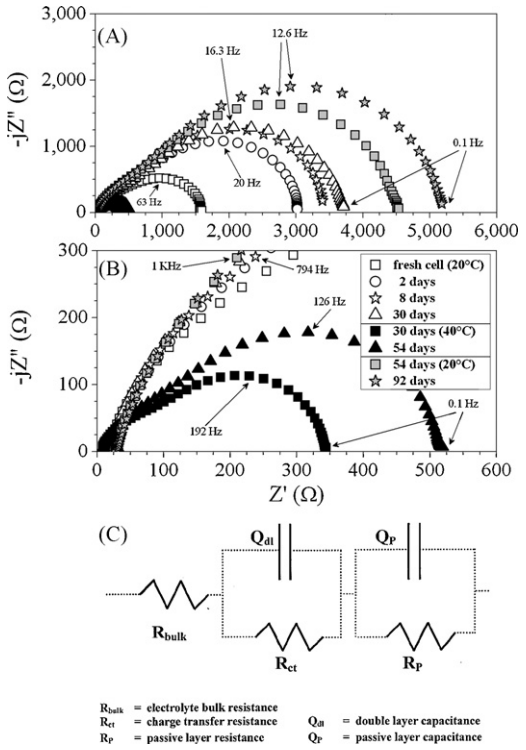

Fig. 8. AC responses of a symmetrical Li/PIL–LiTFSI–PYR_{14}TFSI (set C)/Li cell stored under different temperature conditions (panel A). Panel B magnified the AC plots obtained at 40 °C. Panel C depicts the equivalent circuit model adopted for fitting the AC responses of panels A and B.

commonly observed in solvent-free polymer electrolytes [47–49], is due to the reaction between the lithium electrode and the polymer electrolyte to form a passive layer (SEI) [36] onto the lithium anode that protects the electrode from further reaction. At 40 °C the interfacial resistances decrease about one order of magnitude

Table 3
Electrolyte bulk resistance (R_b), charge transfer resistance (R_{ct}) and passive layer resistance (R_p) values for a PIL–LiTFSI–PYR_{14}TFSI ternary polymer electrolyte (set C) in contact with a lithium anode at different storage times and temperatures. The R_b, R_{ct} and R_p parameters, normalized with respect to the electrochemically active area, were obtained by fitting the impedance measurements of Fig. 8 (panels A and B) using the NLLSQ fit software on the basis of the equivalent circuit model depicted in panel C (Fig. 8).

Time (days)	T (°C)	R_b (Ω)	R_{ct} (Ω cm^2)	R_P (Ω cm^2)
0	20	18 ± 2	270 ± 40	630 ± 90
1	20	18 ± 2	400 ± 60	810 ± 100
2	20	19 ± 2	420 ± 60	1300 ± 200
5	20	20 ± 2	410 ± 60	1500 ± 200
8	20	18 ± 2	420 ± 60	1500 ± 200
13	20	20 ± 2	490 ± 70	1700 ± 200
20	20	18 ± 2	420 ± 60	1500 ± 200
26	20	21 ± 2	500 ± 70	1700 ± 200
30	20	19 ± 2	430 ± 50	1600 ± 200
30	40	5.8 ± 0.4	66 ± 7	120 ± 10
33	40	5.3 ± 0.4	68 ± 7	130 ± 10
37	40	6.0 ± 0.5	70 ± 7	140 ± 10
43	40	6.0 ± 0.5	76 ± 8	160 ± 20
50	40	7.5 ± 0.6	77 ± 8	160 ± 20
54	40	6.4 ± 0.5	84 ± 8	200 ± 20
54	20	21 ± 2	460 ± 50	2000 ± 200
64	20	22 ± 2	500 ± 50	2200 ± 200
71	20	22 ± 2	500 ± 50	2200 ± 200
78	20	20 ± 2	530 ± 50	2100 ± 200
92	20	17 ± 2	500 ± 50	2200 ± 200

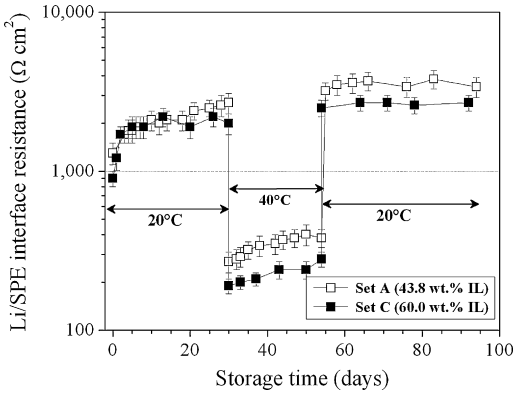

Fig. 9. Time evolution of the interfacial resistance of various PIL–LiTFSI–PYR_{14}TFSI electrolytes in contact with lithium metal anode at different temperatures. The interfacial resistance was normalized with respect to the lithium electrode active area.

(280 Ω cm^2) whereas in the following period at 20 °C the R_i values approach the ones observed during the initial storage. The passive layer and charge transfer resistance values reported in Table 3 show analogous time evolution with respect to R_i. It is to note that the interface resistance is mainly located in the SEI film (Table 3). As clearly evidenced from Fig. 9, the increase of the ionic liquid content leads to a decrease of the interfacial resistance. This behavior, previously observed also in ionic liquid-based PEO electrolytes [26], may be likely ascribed to the capability of the ionic liquid to promote the lithium cation motion through the SEI film. Even if this issue needs to be further clarified, the incorporation of suitable ionic liquids may represent a promising approach for lowering the room temperature interfacial resistance at the interface with the lithium anode, thus enhancing the performance in battery. We are currently approaching this aspect working both on the lithium metal chemistry and on the ionic liquid architecture.

3.6. Lithium stripping/plating

In Fig. 10, panel A, is reported the cell overvoltage vs. time profile of a few selected cycles from a symmetric Li/PIL–LiTFSI–PYR_{14}TFSI (set A)/Li cell (40 °C) subjected to lithium plating-stripping tests. As it is seen in the figure, the cell showed the capability of performing more than 2100 cycles without any major change in the plating and stripping voltage trends. We would like to point out that 1000 cycles correspond to a test period of about 3 months. The maximum overvoltage detected at the end of each plating or stripping half-cycle is reported in panel B of Fig. 10. The cell overvoltage is seen to progressively increase from 60 mV (first cycle) to about 120 mV after more than 2100 cycles, in agreement with the AC plots reported in the inset of panel B. The smooth shape of the overvoltage-time profiles and the low frequency spur inclined straight line (inset of panel B), typical of diffusion process into the electrolyte [36], do not indicate growth of dendrites. No change of the polymer electrolyte ionic resistance is observed, again suggesting no relevant major decomposition within the PIL–LiTFSI–PYR_{14}TFSI electrolytes even after prolonged lithium cycling tests.

3.7. Full battery tests

The PIL–LiTFSI–PYR_{14}TFSI (set C) ternary polymer electrolytes were tested in Li/$LiFePO_4$ all-solid-state batteries at low-medium temperatures (40 °C). Fig. 11, panel A, shows the voltage vs. capacity profile of selected discharge half-cycles obtained at various

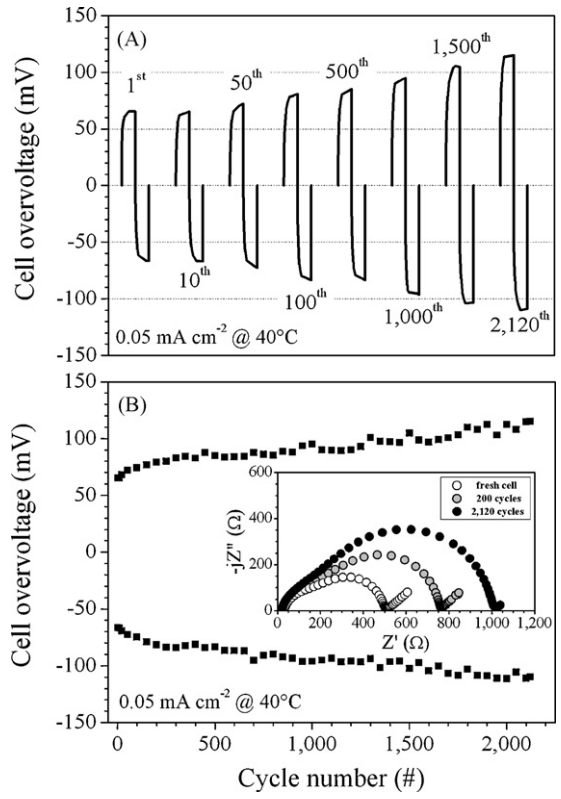

Fig. 10. Selected plating-stripping cycles (panel A) and overvoltage evolution (panel B) measured at the end of each semi-cycle during the cycling of a symmetric Li/PIL–LiTFSI–PYR_{14}TFSI (set A)/Li cell at 40 °C (±1 °C). Current density: 0.05 mA cm^{-2}. Plating and stripping time: 1 h. Lithium electrode: area: 2.0 cm^2; thickness: 0.05 mm. The insert in panel B depicts the result of AC impedance measurements taken on the cell after selected cycles.

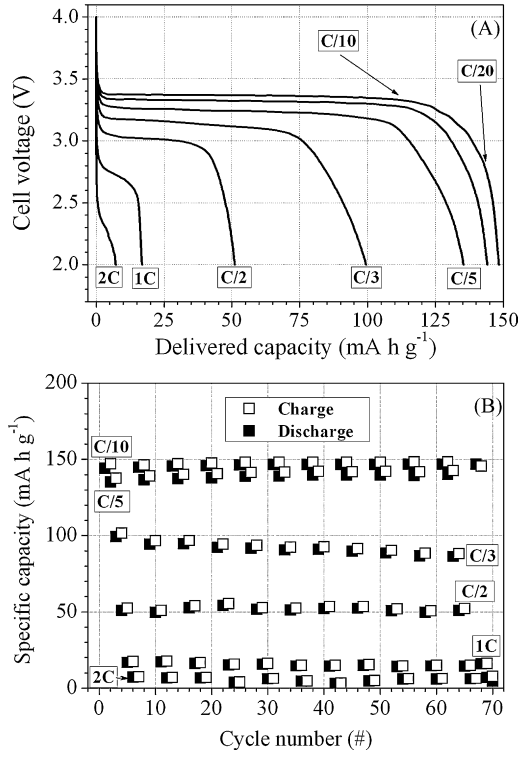

Fig. 11. Voltage vs. capacity profile of selected discharge half-cycles (panel A) and cycling performance (panel B) of a Li/PIL–LiTFSI–PYR_{14}TFSI (set C)/$LiFePO_4$ polymer battery at 40 °C. Charge rate: C/20 (0.044 mA cm^{-2}). The discharge rate was ranged from C/20 to 2C (1.8 mA cm^{-2}).

Table 4
Discharge capacity values for a Li/PIL–LiTFSI–PYR_{14}TFSI(set C)/$LiFePO_4$ full polymer battery at 40 °C and different current rates.

Current rate (C/*n*)	Current density (mA cm^{-2})	Delivered capacity (mAh g^{-1})	Percent of the nominal capacity (%)
C/20	0.044	148.4	87.3
C/10	0.088	144.1	84.8
C/5	0.176	135.3	79.6
C/3	0.293	99.5	58.5
C/2	0.440	51.1	30.1
1C	0.880	16.9	9.9
2C	1.760	7.2	4.2

current rates. The discharge (Li insertion) process is revealed by a 3.4–3.2 V, well-defined, flat plateau, typical of Li/SPE/$LiFePO_4$ batteries [50,51], up to medium discharge rates (C/2–C/3). A progressive feature change of the discharge plateaus and an ohmic drop increase occur at higher current densities.

Panel B of Fig. 11 illustrates the cycling performance of a Li/PIL–LiTFSI–PYR_{14}TFSI (set C)/$LiFePO_4$ battery at 40 °C and different current rates. The results show very good capacity retention during prolonged cycling tests even at high rates (2C). No dramatic decrease in capacity is observed up to C/5, suggesting that the limiting current density is above this value. The batteries are capable of delivering large capacities, i.e., above 140 mAh g^{-1} (82.3% of the theoretical value) up to medium rates (C/5). Under these experimental conditions (e.g., 40 °C@C/5) the performance of the Li/PIL–LiTFSI–PYR_{14}TFSI/$LiFePO_4$ batteries is comparable to that obtained in ionic liquid-free polymer cells operating at medium-high temperatures (70–100 °C) [52]. A good capacity, e.g., 100 mAh g^{-1} corresponding to 58.8% of the nominal capacity, is also discharged at C/3 while moderate values (55 mAh g^{-1}, e.g., 32.3%) are obtained at higher rates (C/2). A further increase of the current rates (≥1C) leads to a capacity performance decay of the Li/$LiFePO_4$ polymer batteries.

Table 4 reports the discharged capacities for a Li/$LiFePO_4$ polymer battery at 40 °C and different current rates. The charge/discharge efficiency was found to level quickly above 98%, this confirms the reversibility of the lithium ion intercalation process as well as the electrochemical stability of the PIL–LiTFSI–PYR_{14}TFSI ternary polymer electrolytes.

4. Conclusions

Solvent-free, ternary polymer electrolytes based on novel poly (diallyldimethylammonium) bis(trifluoromethanesulfonyl)imide polymeric ionic liquid (PIL) as polymer host and incorporating PYR_{14}TFSI ionic liquid and LiTFSI salt were prepared and investigated. The PIL–LiTFSI–PYR_{14}TFSI ternary electrolyte system showed good mechanical properties with high chemical stability even after prolonged storage times in contact with lithium anode and it is thermally stable up to 300 °C. The thermal properties are well correlated with the electrochemical ones. The PIL-based polymer electrolytes exhibited room temperature ionic conductivity above 10^{-4} S cm^{-1} with an electrochemical stability window up to 5.0 V vs. Li^+/Li°, time-stable interfacial resistance values and good lithium stripping/plating performance. The increase of ionic liquid content resulted in a conductivity increase and, at the same time, in a decrease of the interface resistance with the lithium electrode. Preliminary tests have shown that Li/$LiFePO_4$ solid-state batteries are able to deliver more than 140 mAh g^{-1} with very good capacity retention up to medium rates (C/5), this making the PIL–LiTFSI–PYR_{14}TFSI membranes promising candidates as electrolyte separators for LMPBs.

Acknowledgements

The authors wish to thank the financial support of the European Commission within the FP6 STREP Project ILLIBATT (Contract no. NMP3-CT-2006-033181) and the Spanish MEC (CONSOLIDER-INGENIO 2010, HOPE Grant 2007-00007) for the financial support. Süd-Chemie is acknowledged for having kindly provided the $LiFePO_4$ material.

References

[1] J.M. Tarascon, M. Armand, Nature (London) 414 (2001) 359.
[2] R. Frech, S. Chintapalli, P.G. Bruce, C.A. Vincent, Macromolecules 32 (1999) 808.
[3] H. Ohno (Ed.), Electrochemical Aspects of Ionic Liquids, John Wiley & Sons, 2005.
[4] M. Armand, F. Endres, D.R. MacFarlane, H. Ohno, B. Scrosati, Nat. Mater. 8 (2009) 621.
[5] A.I. Bhatt, I. May, V.A. Volkovich, M.E. Hetherington, B. Lewin, R.C. Thied, N. Ertok, J. Chem. Soc., Dalton Trans. 4532 (2002).
[6] S. Panozzo, M. Armand, O. Stephan, Appl. Phys. Lett. 80 (2002) 679.
[7] P. Wang, S.M. Zakeeruddin, I. Exnar, M. Gratzel, Chem. Commun. 2972 (2002).
[8] J. Fuller, A.C. Breda, R.T. Carlin, J. Electroanal. Chem. 459 (1998) 29.
[9] H. Nakagawa, S. Izuchi, K. Kunawa, T. Nukuda, Y. Aihara, J. Electrochem. Soc. 150 (2003) A695.
[10] H. Sakaebe, H. Matsumoto, Electrochem. Commun. 5 (2003) 594.
[11] A. Noda, M.A.B.H. Susan, K. Kudo, S. Mitsushima, K. Hayamizu, M. Watanabe, J. Phys. Chem. B 107 (2003) 4024.
[12] A. Balducci, W.A. Henderson, M. Mastragostino, S. Passerini, P. Simon, F. Soavi, Electrochim. Acta 50 (2005) 2233.
[13] Y.S. Fuang, R.Q. Zhou, J. Power Sources 81 (1999) 891.
[14] J.-H. Shin, W.A. Henderson, S. Passerini, Electrochem. Commun. 5 (2003) 1016.
[15] A. Lewandowski, A. Swiderska, Solid State Ionics 169 (2004) 21.
[16] J.-H. Shin, W.A. Henderson, S. Passerini, Electrochem. Solid-State Lett. 8 (2005) A125.
[17] J.-H. Shin, W.A. Henderson, S. Passerini, J. Electrochem. Soc. 152 (2005) A978.
[18] J.-H. Shin, W.A. Henderson, G.B. Appetecchi, F. Alessandrini, S. Passerini, Electrochim. Acta 50 (2005) 3859.
[19] J.-H. Shin, W.A. Henderson, S. Scaccia, P.P. Prosini, S. Passerini, J. Power Sources 156 (2006) 560.
[20] J.-H. Shin, W.A. Henderson, C. Tizzani, S. Passerini, S.-S. Jeong, K.-W. Kim, J. Electrochem. Soc. 153 (9) (2006) A1649.
[21] D.R. MacFarlane, J. Sun, M. Forsyth, P. Meakin, N. Amini, J. Phys. Chem. B 103 (1999) 4164.
[22] D.R. MacFarlane, J. Huang, M. Forsyth, Nature (London) 402 (1999) 792.
[23] G.B. Appetecchi, M. Montanino, D. Zane, M. Carewska, F. Alessandrini, S. Passerini, Electrochim. Acta 54 (2009) 1325.
[24] Z.B. Zhou, H. Matsumoto, K. Tatsumi, Chem. Eur. J. 12 (2006) 2196.
[25] V.R. Koch, C. Nanjundiah, G.B. Appetecchi, B. Scrosati, J. Electrochem. Soc. 142 (1995) L116.
[26] G.-T. Kim, G.B. Appetecchi, F. Alessandrini, S. Passerini, J. Power Sources 171 (2007) 861.
[27] G.B. Appetecchi, G.-T. Kim, M. Montanino, F. Alessandrini, S. Passerini, ECS Trans. 11 (2008) 119.
[28] R. Marcilla, F. Alcaide, H. Sardon, J.A. Pomposo, C. Pozo-Gonzalo, D. Mecerreyes, Electrochem. Commun. 8 (2006) 482.
[29] N. Matsumi, K. Sugai, M. Miyake, H. Ohno, Macromolecules 39 (2006) 6924.
[30] H. Ohno, Electrochim. Acta 46 (2001) 1407.
[31] M. Yoshizawa, H. Ogihara, H. Ohno, Polym. Adv. Technol. 13 (2002) 589.
[32] A.-L. Pont, R. Marcilla, I. De Meatza, H. Grande, D. Mecerreyes, J. Power Sources 188 (2009) 558.
[33] G.B. Appetecchi, S. Scaccia, C. Tizzani, F. Alessandrini, S. Passerini, J. Electrochem. Soc. 153 (9) (2006) A1685.
[34] B.A. Boukamp, Solid State Ionics 18 (1986) 136.
[35] B.A. Boukamp, Solid State Ionics 20 (1986) 31.
[36] J.R. MacDonald, Impedance Spectroscopy, John Wiley & Sons, New York, 1987.
[37] W.A. Henderson, S. Passerini, Chem. Mater. 16 (2004) 2881.
[38] H. Vogel, Phys. Z. 22 (1921) 645;
G.S. Fulcher, J. Am. Chem. Soc. 8 (1925) 339;
G. Tamman, W. Hesse, Z. Anorg. Allg. Chem. 156 (1926) 245.
[39] S. Lascaud, M. Perrier, A. Valle'e, S. Besner, J. Prud'homme, M. Armand, Macromolecules 27 (1994) 7469.
[40] G.B. Appetecchi, G. Dautzenberg, B. Scrosati, J. Electrochem. Soc. 143 (1996) 6.
[41] Y. Aihara, G.B. Appetecchi, B. Scrosati, J. Electrochem. Soc. 149 (2002) A849.
[42] H. Cheradame, P. Niddam-Mercier, Faraday Discuss. Chem. Soc. 88 (1989) 77.
[43] M.A. Ratner, D.F. Shriver, Mater. Res. Soc. Bull. (1989) 39.
[44] M. Castriota, T. Caruso, R.G. Agostino, E. Cazzanelli, W.A. Henderson, S. Passerini, J. Phys. Chem. A 109 (2005) 92.
[45] I. Nicotera, C. Oliviero, W.A. Henderson, G.B. Appetecchi, S. Passerini, J. Phys. Chem. B 109 (2005) 22814.
[46] S. Passerini, B. Scrosati, J. Electrochem. Soc. 141 (1994) 889.
[47] G.B. Appetecchi, S. Scaccia, S. Passerini, J. Electrochem. Soc. 147 (2000) 4448.
[48] G.B. Appetecchi, F. Alessandrini, M. Carewska, T. Caruso, P.P. Prosini, S. Scaccia, S. Passerini, J. Power Sources 97 (2001) 790.
[49] G.B. Appetecchi, S. Passerini, J. Electrochem. Soc. 149 (2002) A891.
[50] A.K. Padhi, K.S. Nanjundaswamy, J.B. Goodenough, J. Electrochem. Soc. 144 (1997) 1188.
[51] N. Ravel, J.B. Goodenough, S. Besner, M. Gauthier, M. Armand, in: Abstracts of the Electrochemical Society and the Electrochemical Society of Japan Meeting (Abstract 127), vol. 99 (2), 2000.
[52] G.B. Appetecchi, J. Hassoun, B. Scrosati, F. Croce, F. Cassel, M. Salomon, J. Power Sources 124 (2003) 246.